Available online at www.sciencedirect.com
ScienceDirect
Trans. Nonferrous Met. Soc. China 23(2013) 1646−1651
Transactions of Nonferrous Metals Society of China
www.tnmsc.cn

Loading rate sensitivity of nanoindentation creep behavior in a Fe-based bulk metallic glass

Fu XU, Zhi-lin LONG, Xu-hui DENG, Ping ZHANG

College of Civil Engineering and Mechanics, Xiangtan University, Xiangtan 411105, China

Received 10 April 2012; accepted 14 December 2012

Abstract: Effect of loading rate on room temperature creep deformation of $\{[(Fe_{0.6}Co_{0.4})_{0.75}B_{0.2}Si_{0.05}]_{0.96}Nb_{0.04}\}_{96}Cr_4$ bulk metallic glass (BMG) was investigated by performing nanoindentation creep experiments. Experimental results show that the creep displacement of the Fe-based BMG increases with increasing the loading rate. Furthermore, based on an empirical power-law equation, the stress exponent for room temperature creep of this BMG was calculated. As the indentation loading rate increases from 1 mN/s to 50 mN/s, the stress exponent decreases gradually from 28.1 down to 4.9, exhibiting significant indentation loading rate sensitivity. Finally, nanoindentation creep behavior in this Fe-based BMG was demonstrated in terms of free volume and “shear transformation zone” (STZ) theories, which could provide semi-quantitative explanation as for the observed experimental and analytical results.

Key words: bulk metallic glass; nanoindentation; creep; loading rate sensitivity

1 Introduction

Since metallic glasses could be produced in bulk form [1], the mechanical property of the amorphous alloys has become a realistic topic on research for possible structural applications. Although there is growing interest in the mechanical properties of bulk metallic glasses (BMGs), the deformation mechanism is far from being understood due to the very limited plasticity before fracture in uniaxial tensile or compression tests at ambient temperature [2,3]. In recent years, nanoindentation technique has been widely used to investigate the plastic deformation behavior of BMGs at room temperature [4] because of its high resolution in recording load — displacement data. BMGs exhibit obvious plastic deformation as pop-in events on the load —displacement curves during loading in nanoindentation, therefore the mechanism of plastic deformation is attested in terms of the formation and propagation of shear bands [5]. Inspired by the successful application of nanoindentation on studying plastic deformation, some researchers attempted to utilize such technique to investigate time-dependent deformation (i.e., creep) behavior of BMGs [6,7]. Nanoindentation creep experiments at room temperature were initially conducted on BMGs, like Ce-, La-, and Mg-based BMG with a low glass transition temperature (T_g) (and thus the room temperature is 0.7−0.75 T_g) since creep is expected to occur mainly at high reduced temperatures (T/T_g>0.7) where deformation is thought to be homogeneous. Recently, HUANG et al [8,9] and YOO et al [10] have attempted to extend the room-temperature creep analysis to Fe-, Ti-based and CuZr BMGs whose T_g is not so low (T/T_g=0.35−0.43). BMGs with low or high T_g all exhibit creep deformation at room temperature, which experimentally break through the restraint of temperature. Additionally, the creep parameters (such as stress exponent) obtained by nanoindentation technique have been found consistent with those from conventional creep tests for a wide range of materials [11−13]. These consistencies are not only useful to measure nano/micromechanical time-dependent deformation of BMGs, but also give a possible attraction of understanding the deformation mechanisms of the materials by indentation test.

Foundation item: Project (51071134) supported by National Natural Science Foundation of China; Project (2012WK2008) supported by the Planned Science and Technology Project of Hunan Province, China; Project (09A088) supported by Scientific Research Fund of Hunan Provincial Education Department, China; Project (12JJ2024) supported by Provincial Natural Science Foundation of Hunan, China; Project (2011XZX18) supported by Xiangtan University Natural Science Foundation, China
Corresponding author: Zhi-lin LONG; Tel: +86-731-58298287; E-mail: longzl@xtu.edu.cn
DOI: 10.1016/S1003-6326(13)62643-6

During nanoindentation creep tests, loading rate sensitivity of indentation creep deformation and stress exponent, which usually appears in polymers and some crystalline materials, has also been found in BMGs. However, the trends of the stress exponent changes with loading rate found by the authors were controversial. For example, HUANG et al [8] suggested that the stress exponent for the power-law creep of a Fe-based BMG decreases with the loading rate used prior to the holding period, whereas YOO et al [10] observed an opposite trend in $Cu_{50}Zr_{50}$ BMG. Metallic glasses are essentially viscoelastic as other glasses[14] and the stress exponent derived from the steady state of creep and the loading rate sensitivity are the key points to understand the mechanism of creep deformation. Apart from the theoretic interests, the creep of BMGs at room temperature under sub-micrometer contacts is also of great practical significance for various possible applications such as nano-, micro-electromechanical system (NEMS, MEMS)

Considering the above-mentioned, a thorough study of the loading rate sensitivity of the creep behavior of a Fe-based bulk metallic glasses, $\{[(Fe_{0.6}Co_{0.4})_{0.75}B_{0.2}Si_{0.05}]_{0.96}Nb_{0.04}\}_{96}Cr_4$ with a relatively high T_g of 833 K was treated as the goal of this current research. Creep test using nanoindentation technique was adopted as an experimental method at room temperature under loading rates ranging from 1 to 50 mN/s. The influence of loading rate on the creep strain rate and stress exponent was demonstrated and the creep deformation mechanism during nanoindentation was discussed as well.

2 Experimental

The ingots of master alloy with nominal composition $\{[(Fe_{0.6}Co_{0.4})_{0.75}B_{0.2}Si_{0.05}]_{0.96}Nb_{0.04}\}_{96}Cr_4$ (mole fraction, %) were prepared by arc melting the mixture of pure Fe, Co, Cr and Nb metals with pure B and Si crystals in a purified argon atmosphere. The ingots were melted at least three times in an arc melter in order to obtain chemical homogeneity. Cylindrical rods of 3 mm in diameter and 40 mm in length were fabricated by copper mold casting. In all cases, the amorphous structure of the alloy was monitored by X-ray diffraction (XRD) with Cu K_α radiation. Thermal stability associated with T_g, crystallization temperature (T_x) and supercooled liquid region $\Delta T_x(=T_x-T_g)$ was evaluated by differential scanning calorimetry (DSC) at a heating rate of 0.67 K/s.

Prior to nanoindentation experiments, the cylindrical rods were cut into 5 mm-thick cylinders and the surfaces of samples were mechanically polished to a mirror finish. The nanoindentation tests were conducted using a triboIndenter from Hysitron Inc. with a standard Berkovich diamond indenter. The load and displacement resolutions of the machine were 100 nN and 0.1 nm, respectively. The machine compliance calibration for the transducer-tip configuration and tip area functional calibration were performed with a standard fused silica sample before proceeding with all indentation experiments. Experiments at constant loading rates of 1, 5, 10, 20 and 50 mN/s were carried out to a load limit of 50 mN followed by a holding period of 40 s. At least four indentation tests were carried out under each condition. Given the time required to conduct the vast majority of the indentation creep experiments, any assumption about the constancy of thermal drift during the entire experiment deserved questioning. With this in mind, every effort was made to minimize the effects of thermal drift in all of the experiments by allowing several hours for thermal equilibrium at each temperature.

3 Results and discussion

Figure 1 shows the XRD pattern and DSC curve of the as-cast Fe-based BMG sample. The as-cast alloy exhibits an XRD spectrum typical for an amorphous phase without an obvious crystalline peak, and T_g, T_x and ΔT_x for this BMG measured by DSC are 833, 874 and 41 K, respectively.

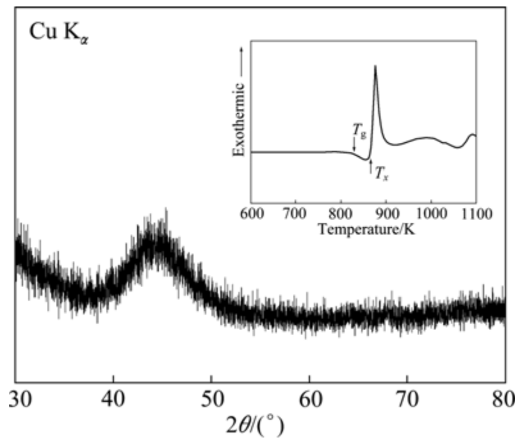

Fig. 1 XRD pattern for as-cast $\{[(Fe_{0.6}Co_{0.4})_{0.75}B_{0.2}Si_{0.05}]_{0.96}Nb_{0.04}\}_{96}Cr_4$ (Inset is DSC curve for alloy)

Figure 2(a) represents the typical load — displacement (P — h) curves during nanoindentation under loading rates ranging from 1 to 50 mN/s at a load limit of 50 mN, and the origin of each curve has been offset for clarity. At each loading rate, the data derived from more than four independent indentations were averaged to minimize the influence of noises, discarding those results biased significantly against the others. The recorded creep displacement curves during the constant load holding are shown in Fig. 2(b). It can be readily observed that during the load holding period, the indenter displacement initially increases sharply with time, followed by a decreasing strain rate, and then exhibits a steady-state behavior, namely, the strain increases linearly with time. Moreover, the magnitude of creep deformation increases with increasing the loading rate, indicating strong loading rate sensitivity. In other words, the materials exhibit better creep resistance (less sensitive to the applied holding load) at a lower loading rate than at a higher one. Similar observation was also reported on $Pd_{40}Cu_{30}Ni_{10}P_{20}$ [7], $Fe_{41}Co_7Cr_{15}Mo_{14}C_{15}B_6Y_2$ [8] and $Cu_{50}Zr_{50}$ [10] BMGs during nanoindentation at room temperature, as well as in some crystalline materials.

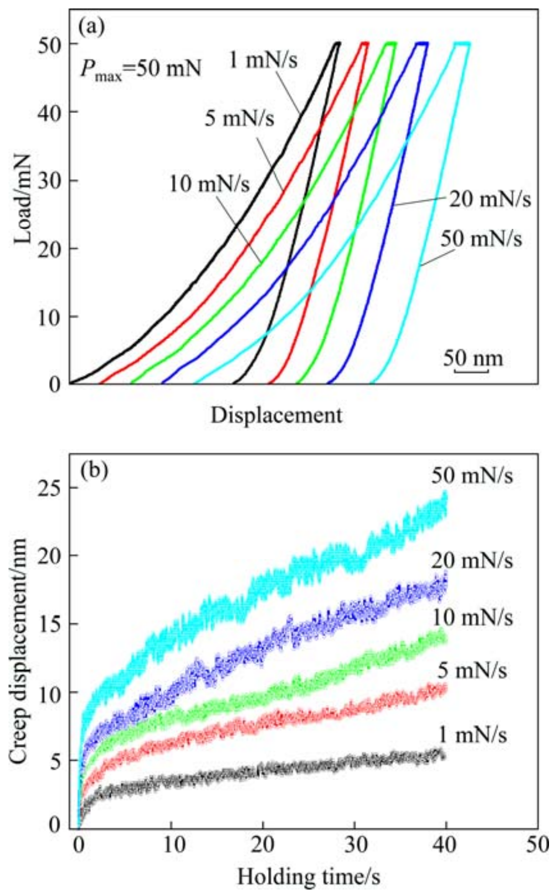

Fig. 2 Typical load—displacement (P—h) curves during nanoindentation under different loading rates and curves offset from origin for clear viewing (a) and recorded creep displacement curves during constant load holding period (b)

For depth-sensing indentation with a self-similar indenter, the dimensional analysis shows that the strain rate can be formulated as the following scaling relation[15]:

$$\dot{\varepsilon} = \frac{1}{h}\frac{\mathrm{d}h}{\mathrm{d}t} \tag{1}$$

where h is the instantaneous indentation displacement and t the indentation time. In fact, this nanoindentation strain rate $\dot{\varepsilon}$ can be computed by taking the slope of the displacement — time curve, i.e. the instantaneous displacement h, and by dividing it by the displacement at any particular point in time. However, due to the fact that the load — displacement data from nanoindentation measurements are scattered, the use of raw nanoindentation data to determine $\dot{\varepsilon}$ can introduce errors. The errors, however, can be reduced by using appropriate curve fitting technique to cast the nanoindentation data into smooth functions such as the following empirical law[16]:

$$h(t) = h_0 + a(t - t_0)^b + kt \tag{2}$$

where h_0 is the initial indentation depth; a, b and k are fitting constants; t_0 is the start time of the creep process. The fitting protocol in Eq. (2) is found to produce very good fit to most of our results, as can be seen from the examples shown in Fig. 3(a) which was obtained at a loading rate of 20 mN/s and peak load of 50 mN. The corresponding creep strain rate $\dot{\varepsilon}$ was calculated by Eq. (1) and also plotted in Fig. 3(a). At the beginning of the load holding period, the penetration deepened at a very high strain rate between 0.1 and 0.001 s^{-1}, the so-called “transient creep”. As steady state was attained, the strain rate gradually saturated at the order of about 10^{-4}. In order to view the effect of loading rate on creep

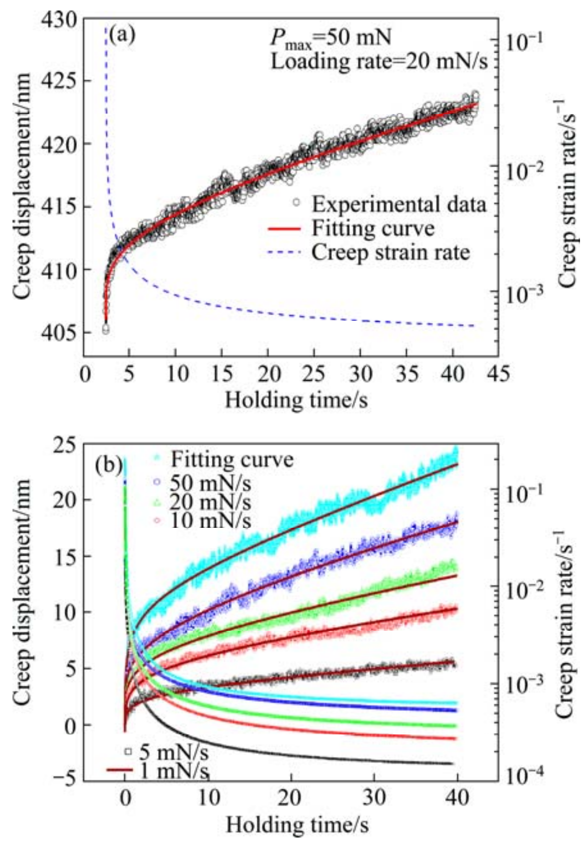

Fig. 3 Experimental creep data, fitting curve and strain rate of sample with loading rate of 20 mN/s (a) and ranging from 1 to 50 mN/s for comparison (b)

clearly, Fig. 3(b) shows the creep fitting curves and the creep stain rates at all the experimental loading rates. To facilitate comparison, the starting points for different loading rate were aligned. It is found that all displacement increases at a declining rate with time and finally reaches an almost constant displacement rate, resulting in a decreasing strain rate against time and displacement. It can also be seen by comparing the results in Fig. 3(b) that at the same holding load, a faster loading corresponds to a higher steady indentation creep strain rate, which shows a clear strong rate dependency.

For steady-state creep behavior, the relationship between the strain rate $\dot{\varepsilon}$ and characteristic stress σ can be described by an empirical power-law equation, which has been verified by theoretical calculations and experimental studies [17−19], i.e.,

$$\dot{\varepsilon} = C\sigma^n \tag{3}$$

where the pre-factor C contains the temperature dependence through the Boltzmann factor; the stress exponent n, which is given by the slope of the lg−lg plot of $\dot{\varepsilon}$ versus σ under isothermal conditions, can provide useful information on the mechanism of the time-dependent deformation concerned. In depth-sensing indentation with the self-similar indenter, the characteristic stress σ (or the hardness) obeys the following scaling relation [20]:

$$\sigma \sim \frac{P}{h^2} \tag{4}$$

where P and h are the instantaneous load and displacement, respectively. As we can see from Fig. 2(b) and Fig. 3 in this study, after holding the peak load for about 5 s, the nanoindentation creep was assumed to be steady, during which the relationship of creep strain rate and characteristic stress is governed by Eq. (3). As an example, Fig. 4(a) shows the plot of $\ln\dot{\varepsilon}$ vs $\ln\sigma$ for the same test as that shown in Fig. 3(a). The slope of the curve n, i.e., $\partial(\ln\dot{\varepsilon})/\partial(\ln\sigma)$, becomes steady towards the end of the holding period (corresponding to the very left region of the curve) and is taken as the stress exponent of the power-law creep described according to Eq. (2). Figure 4(b) shows the stress exponent variation as a function of the indentation loading rate. With increasing the loading rate from 1 to 50 mN/s, the estimated stress exponent in the steady-state region decreases gradually from 28.1 to 4.9, indicating a strong dependence on the indentation loading rate. The trend of the stress exponent changing with the loading rate in the present study is consistent with the results by HUANG et al [8]. However, the values of stress exponent obtained by them from $Fe_{41}Co_7Cr_{15}Mo_{14}C_{15}B_6Y_2$ BMG (0.94 to 4.93) [8] are smaller than those by us (4.9 to 28.1). Such discrepancies can be attributed to the fact that a larger peak load usually causes a larger stress exponent, which has been demonstrated by many works. Note that the peak load in this study (50 mN) is five times the value used by HUANG et al [8] (10 mN).

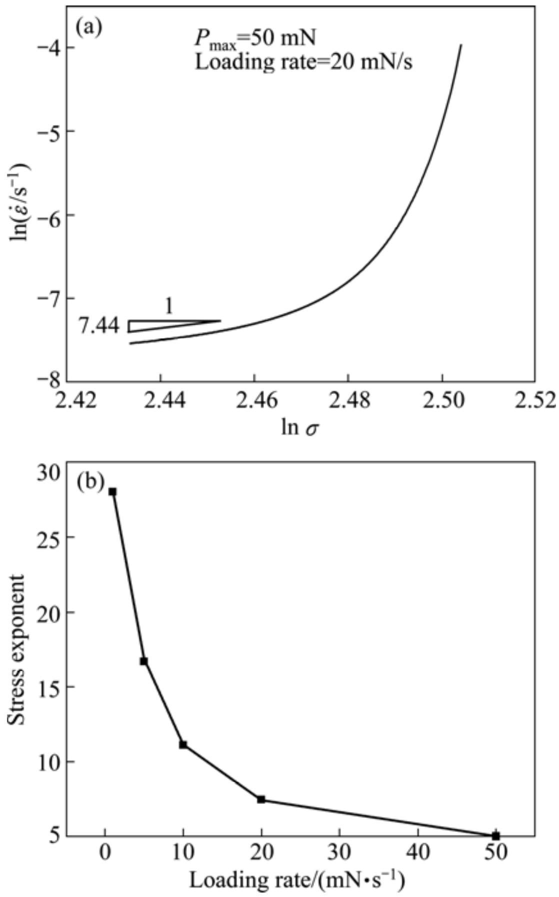

Fig. 4 Corresponding $\ln\dot{\varepsilon}$ versus $\ln\sigma$ plot for data shown in Fig. 3(b) (a) and variation of steady-state stress exponent with indentation loading rates (b)

Plastic deformation of metallic glasses occurs by the superposition of the shear of localized groups of atoms, and often is referred to as "flow defects" on "shear transformation zones" (STZs) [21]. The defects in amorphous metals are often described by the free volume model, in which they appear as density fluctuation with volume greater than critical value v^*. The concentration of the free volume is described by [22]

$$c_{\rm f} = \exp(-\frac{\gamma v^*}{v_{\rm f}}) \tag{5}$$

where γ is a geometrical factor between 0.5 and 1, and $v_{\rm f}$ is the average free volume of an atom. When subjected to an external stress σ, small region of volume v_0 undergoes a strain ε_0 at a rate that depends on the stress. The macroscopic uniaxial strain rate $\dot{\varepsilon}_{\rm u}$ can be formulated as

$$\dot{\varepsilon}_{\rm u} = 2c_{\rm f}k_{\rm f}\frac{\varepsilon_0 v_0}{\Omega}\sinh(\frac{\sigma\varepsilon_0 v_0}{2kT}) \tag{6}$$

where Ω is the atomic volume; k is Boltzmann's constant; T is the temperature; k_f is a temperature-dependent rate constant.

For nanoindentation tests, the indentation strain rate $\dot{\varepsilon}$ can be related to the effective uniaxial strain rate $\dot{\varepsilon}_u$ by $\dot{\varepsilon}_u = 0.09\dot{\varepsilon}$ [4]. The relation of the indentation strain rate $\dot{\varepsilon}$ and the concentration of the free volume c_f is therefore obtained as

$$\dot{\varepsilon}_i = 0.18Ac_f \tag{7}$$

with

$$A = k_f \frac{\varepsilon_0 v_0}{\Omega}\sinh(\frac{\sigma\varepsilon_0 v_0}{2kT})$$

Based on the results of KIM et al [23], the change of temperature can be omitted during nanoindentation process. Hence, A is constant in nanoindentation test for the same sample and the concentration of free volume is proportional to the strain rate. Combining this with creep strain rate given in Fig. 3(b), we may draw a conclusion that during the load holding period, the higher the loading rate used prior to the creeping segment(with higher creep strain rate), the greater the concentration of free volume. As a result, the specimen may exhibit more macroscopically viscous flow behavior since the viscosity is inversely proportional to the free volume concentration. This is evidenced by the reduction of the stress exponent at higher loading rates, as shown in Fig. 4(b). Furthermore, SPAEPEN [22] suggested that, at a sufficiently high stress, an atom with hard-sphere volume υ^* can be squeezed into a neighbouring hole with a smaller volume υ. This makes the neighbours of the new position move out, and creates a certain amount of free volume. The amount of free volume created per second $\Delta^+\upsilon_f$ is given by

$$\Delta^+\upsilon_f = \frac{\gamma\upsilon^*}{\upsilon_f}\frac{2kT}{S}\left[\cosh(\frac{\sigma\varepsilon_0\upsilon_0}{2kT})-1\right]Nk_f\exp(-\frac{\gamma\upsilon^*}{\upsilon_f}) \tag{8}$$

where N and S are the total number of atoms and the material constant, respectively. Thus, combining Eq. (6) with Eq. (8), in which the hyperbolic functions can approximate to exponentials due to high stress state, gives

$$\Delta^+\upsilon_f = 0.09B\dot{\varepsilon} \tag{9}$$

where

$$B = \frac{NkT}{S}\frac{\gamma\upsilon^*}{\upsilon_f}\frac{\Omega}{\varepsilon_0 v_0}$$

Equation (9) indicates that the production rate of free volume during deformation is proportional to the strain rate. It is consistent with the result of HEY et al [24] by DSC measurements that the free volume after deformation increases with increasing the strain rate. Since the creep strain rate with a higher loading rate is increased as shown in Fig. 3(b), more free volume will be created during the load holding period, resulting in a more homogeneous deformation and a smaller stress exponent.

Next, let's focus on the effect of the loading history on structural state of the specimen. By utilizing Eq. (1), the loading rate was converted to the strain rate presented in Fig. 5. Enlighten by Eq. (9), we may also know that a material indented at a higher strain rate will generate a larger amount of excess free volume during the loading sequence. On the other hand, this may be a explanation of the results that faster loading before the load holding period responds to higher concentration of free volume during steady flow segment as mentioned above. According to STZ theory [25], a BMG with more amount of free volume created, which makes the movement and rearrangement of STZs easier, will generate more STZs under stress in local region, and thus will be less resistant to time-dependent deformation. Therefore, more pronounced creep deformation is reasonable at a higher loading rate, as the experimental results shown in Fig. 2. Figure 5 also illustrates that the strain rate decreases as ~$1/h$, approaching an approximately constant value for very large depths. The trends in strain rate are not monotonic, but exhibit many serrations in strain rate which appear to increase in size as the indentation proceeds, which is consistent with that observed by SCHUH [4] but beyond the scope of this work. Detailed discussion about the loading rate effects on the serrations is appreciated to be found in Ref. [4].

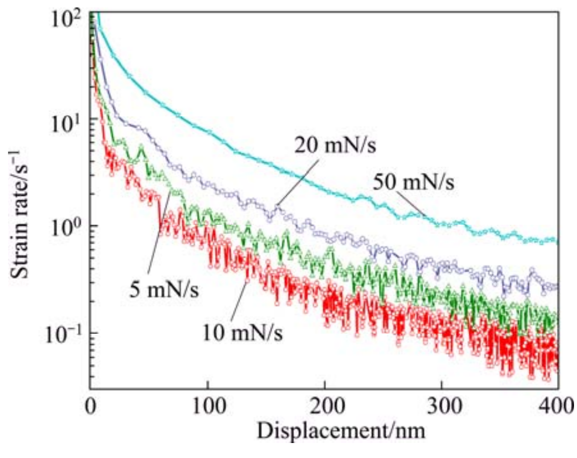

Fig. 5 Indentation strain rate vs depth at different loading rates

4 Conclusions

1) Creep deformation of $\{[(Fe_{0.6}Co_{0.4})_{0.75}B_{0.2}Si_{0.05}]_{0.96}Nb_{0.04}\}_{96}Cr_4$ BMG was investigated through nanoindentation test. The magnitude of the creep displacement increases with increasing the loading rate.

2) As the indentation loading rate increases from

1 mN/s to 50 mN/s, the stress exponent decreases gradually from 28.1 down to 4.9, exhibiting significant indentation loading rate sensitivity. The stress exponent decreases with increasing the loading rate, indicating that plastic flow at higher loading rates is more homogeneous than at smaller loading rates.

3) The creep deformation mechanism was discussed in light of the free volume and “shear transformation zone” (STZ) theories, which provides semi-quantitative explanation for the observed experimental results.

References

[1] CHEN H S. Thermodynamic considerations on the formation and stability of metallic glasses [J]. Acta Metallurgica, 1974, 22(12): 1505−1511.

[2] MUKAI T, NIEH T G, KAWAMURA Y, INOUE A, HIGASHI K. Dynamic response of a $Pd_{40}Ni_{40}P_{20}$ bulk metallic glass in tension [J]. Scripta Materialia, 2002, 46(1): 43−47.

[3] LONG Z L, SHAO Y, XIE G Q, ZHANG P, SHEN B L, INOUE A. Enhanced soft-magnetic and corrosion properties of Fe-based bulk glassy alloys with improved plasticity through the addition of Cr [J]. Journal of Alloys and Compounds, 2008, 462(1−2): 52−59.

[4] SCHUH C A, NIEH T G. A nanoindentation study of serrated flow in bulk metallic glasses [J]. Acta Materialia, 2003, 51(1): 87−99.

[5] GREER A L, CASTELLERO A, MADGE S V, WALKER I T, WILDE J R. Nanoindentation studies of shear banding in fully amorphous and partially devitrified metallic alloys [J]. Materials Science and Engineering A, 2004, 375−377: 1182−1185.

[6] LI W H, SHIN K, LEE C G, WEI B C, ZHANG T H, HE Y Z. The characterization of creep and time-dependent properties of bulk metallic glasses using nanoindentation [J]. Materials Science and Engineering A, 2008, 478(1−2): 371−375.

[7] CONCUSTELL A, SOTT J, GREER A L, BARó M D. Anelastic deformation of a $Pd_{40}Cu_{30}Ni_{10}P_{20}$ bulk metallic glass during nanoindentation [J]. Applied Physics Letters, 2006, 88(17): 171911.

[8] HUANG Y J, SHEN J, CHIU Y L, CHEN J J J, SUN J F. Indentation creep of an Fe-based bulk metallic glass [J]. Intermetallics, 2009, 17(4): 190−194.

[9] HUANG Y J, CHIU Y L, SHEN J, CHEN J J J, SUN J F. Indentation creep of a Ti-based metallic glass [J]. Journal of Materials Research, 2009, 24(3): 978−982.

[10] YOO B G, OH J H, KIM Y J, PARK K W, LEE J C, JANG J I. Nanoindentation analysis of time-dependent deformation in as-cast and annealed Cu−Zr bulk metallic glass [J]. Intermetallics, 2010, 18(10): 1898−1901.

[11] LI J C M. Impression creep and other localized tests [J]. Materials Science and Engineering A, 2002, 322(1−2): 23−42.

[12] LUCAS B N, OLIVER W C. Indentation power-law creep of high-purity indium [J]. Metallurgical and Materials Transactions A, 1999, 30(3): 601−610.

[13] WANG C L, LAI Y H, HUANG J C, NIEH T G. Creep of nanocrystalline nickel: A direct comparison between uniaxial and nanoindentation creep [J]. Scripta Materialia, 2010, 62(4): 175−178.

[14] DMOWSKI W, IWASHITA T, CHUANG C P, ALMER J, EGAMI T. Elastic heterogeneity in metallic glasses [J]. Physical Review Letters, 2010, 105(20): 205502.

[15] MAYO M J, NIX W D. A micro-indentation study of superplasticity in Pb, Sn, and Sn−38wt% Pb [J]. Acta Metallurgica, 1988, 36(8): 2183−2192.

[16] LI H, NGAN A H W. Size effects of nanoindentation creep [J]. Journal of Materials Research, 2004, 19(2): 513−522.

[17] STORAKERS B, LARSSON P L. On Brinell and Boussinesq indentation of creeping solids [J]. Journal of the Mechanics and Physics of Solids, 1994, 42(2): 307−332.

[18] LI W B, HENSHALL J L, HOOPER R M, EASTERLING K E. The mechanisms of indentation creep [J]. Acta Metallurgica et Materialia, 1991, 39(12): 3099−3110.

[19] CHANG H, ALTSTETTER C J, AVERBACK R S. Characteristics of nanophase TiAl produced by inert gas condensation [J]. Journal of Materials Research, 1992, 7(11): 2962−2970.

[20] LIU Y, LIN I K, ZHANG X. Mechanical properties of sputtered silicon oxynitride films by nanoindentation [J]. Materials Science and Engineering A, 2008, 489(1−2): 294−301.

[21] HEGGEN M, SPAEPEN F, FEUERBACHER M. Creation and annihilation of free volume during homogeneous flow of a metallic glass [J]. Journal of Applied Physics, 2005, 97(3): 033506.

[22] SPAEPEN F. A microscopic mechanism for steady state inhomogeneous flow in metallic glasses [J]. Acta Metallurgica, 1977, 25(4): 407−415.

[23] KIM J J, CHOI Y, SURESH S, ARGON A S. Nanocrystallization during nanoindentation of a bulk amorphous metal alloy at room temperature [J]. Science, 2002, 295(5555): 654−657.

[24] de HEY P, SIETSMA J, van den BEUKEL A. Structural disordering in amorphous $Pd_{40}Ni_{40}P_{20}$ induced by high temperature deformation [J]. Acta Materialia, 1998, 46(16): 5873−5882.

[25] ARGON A S. Plastic deformation in metallic glasses [J]. Acta Metallurgica, 1979, 27(1): 47−58.

一种铁基块体金属玻璃纳米压痕蠕变行为的加载速率敏感性

许 福，龙志林，邓旭辉，张 平

湘潭大学 土木工程与力学学院，湘潭 411105

摘　要：通过纳米压痕蠕变实验研究了加载速率对$\{[(Fe_{0.6}Co_{0.4})_{0.75}B_{0.2}Si_{0.05}]_{0.96}Nb_{0.04}\}_{96}Cr_4$ 块体金属玻璃室温蠕变变形的影响。结果表明，该铁基块体金属玻璃的蠕变变形随着加载速率的增加而增大。此外，根据经验幂率函数计算得到了材料室温蠕变应力指数，当加载速率从 1 mN/s 增加到 50 mN/s 时，应力指数从 28.1 逐渐下降到 4.9，显示出显著的压痕加载速率敏感性。最后，基于自由体积理论和剪切转变区理论对该铁基块体金属玻璃的纳米压痕蠕变行为进行了探讨，并对实验结果和分析结果提供了半定量的解释。

关键词：块体金属玻璃；纳米压痕；蠕变；加载速率敏感性

(Edited by Hua YANG)